Revisiting the Role of Mountains in the Northern Hemisphere Winter Atmospheric Circulation

R. H. WHITE,[a] J. M. WALLACE,[b] AND D. S. BATTISTI[b]

[a] *Department of Earth, Ocean and Atmospheric Sciences, University of British Columbia, Vancouver, British Columbia, Canada*
[b] *Department of Atmospheric Sciences, University of Washington, Seattle, Washington*

(Manuscript received 30 September 2020, in final form 9 April 2021)

ABSTRACT: The impact of global orography on Northern Hemisphere wintertime climate is revisited using the Whole Atmosphere Community Climate Model, version 6 (WACCM6). A suite of experiments explores the roles of both resolved orography and the parameterized effects of unresolved orographic drag (hereafter *parameterized orography*), including gravity waves and boundary layer turbulence. Including orography reduces the extratropical tropospheric and stratospheric zonal mean zonal wind $\overline{U}$ by up to 80%; this is substantially greater than previous estimates. Ultimately, parameterized orography accounts for 60%–80% of this reduction; however, away from the surface most of the forcing of $\overline{U}$ by parameterized orography is accomplished by *resolved* planetary waves. We propose that a catalytic wave–mean-flow positive feedback in the stratosphere makes the stratospheric flow particularly sensitive to parameterized orography. Orography and land–sea contrast contribute approximately equally to the strength of the midlatitude stationary waves in the free troposphere, although orography is the dominant cause of the strength of the Siberian high and Aleutian low at the surface and of the position of the Icelandic low. We argue that precisely quantifying the role of orography on the observed stationary waves is an almost intractable problem, and in particular should not be approached with linear stationary wave models in which $\overline{U}$ is prescribed. We show that orography has less impact on stationary waves, and therefore on $\overline{U}$, on a backward-rotating Earth. Last, we show that atmospheric meridional heat transport shows remarkable constancy across our simulations, despite vastly different climates and stationary wave strengths.

KEYWORDS: Atmosphere; Northern Hemisphere; Atmospheric circulation; Stationary waves; Stratospheric circulation; General circulation models

1. Introduction

Since the middle of the twentieth-century orography has been known to have a substantial impact on large-scale circulation and stationary waves (Charney and Eliassen 1949; Bolin 1950). Orography subsequently affects regional climates around the world, as reflected in the climatology of surface temperatures (Seager et al. 2002) and precipitation (Broccoli and Manabe 1992; Wills and Schneider 2015). Traditionally the North American Cordillera (or Rocky Mountains) and the Tibetan Plateau and Himalaya have been considered the most important topographic features influencing atmospheric flow (e.g., Held et al. 2002). However, recent work suggests that the smaller Mongolian plateau to the north of the Himalaya is the most important region of Northern Hemisphere (NH) orography during boreal winter, due to its location within the latitude of strong near-surface zonal winds (White et al. 2017, 2018).

Earth's atmospheric stationary waves are manifest in the planetary-scale wavelike structures in climatological sea level pressure or geopotential height. In the NH the dominant features of the wintertime stationary waves are so prominent they have been given names: the Aleutian low, the Icelandic low, and the Siberian high. The forcing of stationary waves is mainly by orography (Charney and Eliassen 1949; Bolin 1950) and zonal asymmetries in atmospheric diabatic heating associated with land–sea temperature contrasts (e.g., Smagorinsky 1953; Manabe and Terpstra 1974; Hoskins and Karoly 1981; Valdes and Hoskins 1991). In addition, orography can also influence diabatic heating, affecting the stationary waves (Chang 2009). Surface heat fluxes associated with ocean currents can also play a modifying role (Garfinkel et al. 2020).

From the 1980s to 2010 numerous studies examined the relative contributions of "orographic" and "thermal" forcing to the observed stationary waves, attempting to quantify the role of orography. This research, collectively using linear and nonlinear stationary wave models, as well as full general circulation models (GCMs), finds that orography produces anywhere between 30% and 66% of the observed stationary wave amplitude (Held 1983; Chen and Trenberth 1988a,b; Nigam et al. 1988; Valdes and Hoskins 1989), with recent estimates toward the lower end of this range (Ting et al. 2001; Held et al. 2002; Chang 2009). The large range of results can be at least partially understood from differences in the background flow into which the orography was placed, including differences in low-level winds (Valdes and Hoskins 1989; Held and Ting

Denotes content that is immediately available upon publication as open access.

Supplemental information related to this paper is available at the Journals Online website: https://doi.org/10.1175/JAS-D-20-0300.s1.

Corresponding author: R. H. White, rachel.white@cantab.net

DOI: 10.1175/JAS-D-20-0300.1

1990; Ringler and Cook 1995; Held et al. 2002), as well as model differences in atmospheric dissipation strength and imposed drag (Valdes and Hoskins 1989). Additionally, as suggested by Held et al. (2002) and shown by Chang (2009), orography impacts the patterns of atmospheric diabatic heating, and thus a separation of the stationary waves into contributions from ''orography'' and ''thermal'' forcing is not a well-posed problem. Indeed, using an intermediate complexity GCM Garfinkel et al. (2020) show that such strong nonlinearities exist between different forcing mechanisms of the stationary waves, that, over the Pacific, the linear addition of the sources gives a response of different sign to the full nonlinear result. Garfinkel et al. (2020) also show that zonal asymmetries in ocean heat fluxes play a small, but not insignificant, role through their influence on the distribution of sea surface temperatures (SSTs). Using a comprehensive GCM Brayshaw et al. (2008, 2009) explored the influence of idealized landmasses (e.g., rectangular continents), orography (e.g., Gaussian shaped mountains), and SST gradients. In this study we focus only on the influence of present-day orography versus land–sea contrast.

In comparison with stationary waves, less attention has been paid to the impact of orography on the axisymmetric (zonal mean) flow. Held et al. (2002) notes that the structure of the tropospheric zonal mean zonal wind $\overline{U}$, in particular the subtropical tropospheric jets, is broadly similar between the Northern Hemisphere and Southern Hemisphere (SH), suggesting that the orography of the NH has relatively little impact in the troposphere. This is consistent with early modeling results (Manabe and Terpstra 1974). Conversely, a strong asymmetry exists between the wintertime zonal mean stratospheric jets in each hemisphere, caused by large differences in planetary wave activity generated by land–sea contrasts and orography (Waugh and Polvani 2010; White et al. 2018). Early modeling results suggested that orography reduces the speed of the NH winter stratosphere jet by approximately 15% (Manabe and Terpstra 1974); however, using a modern GCM White et al. (2018) find that the presence of the ''Mongolian mountains'' of Asia alone reduces stratospheric $\overline{U}$ in winter by up to 40%. The parameterization of the sub-grid-scale orography, which has been much improved in recent models, has been shown to be critical for correctly simulating the effects of orography on the zonal mean wind (Palmer et al. 1986; Sandu et al. 2016) as well as the general circulation, including stationary waves (Wallace et al. 1983; Sigmond and Scinocca 2010).

Multiple mechanisms exist for how orography impacts the stationary waves and axisymmetric flow. Orography acts as a large-scale obstruction to the flow, creating stationary waves (Charney and Eliassen 1949; Bolin 1950); these stationary waves can also influence the axisymmetric flow through wave–mean-flow interactions (Eliassen and Palm 1961; Charney and Drazin 1961; Andrews and McIntyre 1976; Edmon et al. 1980). Other impacts of orography on the circulation that are at least partially resolved in models include orographic pressure torque, created by gradients in pressure between the western and eastern flanks of mountains (e.g., Wahr and Oort 1984), and differential heating (both radiative and latent) caused by orography (e.g., Ringler and Cook 1995; Wills and Schneider 2018). Orography also affects circulation through sub-grid-scale impacts that must be parameterized at the resolution of past and current GCMs (e.g., Wallace et al. 1983; Boer et al. 1984). Sandu et al. (2016) give a thorough description of the sub-grid-scale effects of orography and their typical representation in atmospheric models. In short, parameterized physics typically include: the forcing of gravity waves, which break close to the surface as well as in the upper atmosphere affecting the circulation (e.g., Boer et al. 1984; McFarlane 1987; Miller et al. 1989; Shaw et al. 2009) and the deceleration of the near-surface flow by turbulent or frictional small-scale processes, including sub-grid-scale blocking of flow (e.g., Webster et al. 2003; Pithan et al. 2016; Sandu et al. 2019). Parameterizing the sub-grid-scale effects of orographic affects both atmospheric $\overline{U}$ (Richter et al. 2010; Sandu et al. 2016; Lindvall et al. 2017; van Niekerk et al. 2018) and the stationary waves (e.g., Wallace et al. 1983; Sigmond and Scinocca 2010; van Niekerk et al. 2017; Sandu et al. 2019). The representation of such processes within GCMs has improved in recent years, through both increased resolution and improved parameterizations (e.g., Beljaars et al. 2004; Garcia et al. 2007; Richter et al. 2010; Garcia et al. 2017), although limitations and biases still exist (Sandu et al. 2019). Given such model improvements, the time seems ripe to reevaluate the role that orography plays in the wintertime climate using a state-of-the-art climate model.

We perform a comprehensive series of experiments using NCAR's Whole Atmosphere Community Climate Model, version 6 (WACCM6), in which global mountains are removed, with and without the simultaneous removal of sub-grid-scale orography. Setting the sub-grid-scale orography to zero removes the effects of unresolved orographic drag parameterized in WACCM6, including gravity waves, nonlinear surface drag, and turbulent form drag; hereafter, we refer to this as the response to ''parameterized orographic drag,'' or, for brevity, ''parameterized orography.'' We quantify the role of both resolved and parameterized orography on the wintertime (December–February in the NH) axisymmetric flow and stationary waves. We briefly discuss the sensitivity to the treatment of sea surface temperatures in section 4. Through analysis of additional mountain/no-mountain experiments in simulations in which Earth is rotated backward, we highlight the strong sensitivity of the orographic response to rotation direction, showing that the current distribution of orography on our planet relative to the coastlines seems to produce a particularly strong orographic response.

2. Models and experiments

We use the WACCM6, a dynamical atmosphere model with 70 vertical levels, including a well-resolved stratosphere (Gettelman et al. 2019). In addition to high vertical resolution in the upper atmosphere, the WACCM has sophisticated parameterizations of the drag from unresolved orography (Gettelman et al. 2019). Effects of unresolved orography are parameterized by two separate schemes: a turbulent orographic form drag (TOFD) scheme, which parameterizes the boundary layer form drag (Beljaars et al. 2004), and a scheme, which parameterizes the effects of gravity wave drag on both

the near-surface and upper atmosphere, and incorporates near-surface nonlinear drag processes (Scinocca and McFarlane 2000). These parameterizations, although sophisticated, remain estimates of the true impact of unresolved orography. In addition to gravity waves forced by sub-grid-scale orography, the WACCM6 includes parameterization of frontal and convectively generated gravity waves (Gettelman et al. 2019; Richter et al. 2010).

For our main simulations a horizontal resolution of 0.9° × 1.25° (hereafter ~1°) is used. All simulations have atmospheric constituent values of the present day (circa year 2000), and the SSTs are fixed to a seasonally varying observed climatology from the late twentieth century (Hurrell et al. 2008). The WACCM6 model reproduces tropospheric and stratospheric circulations well, including stratospheric variability in the form of sudden stratospheric warmings (Gettelman et al. 2019). Throughout this paper we further evaluate the WACCM by comparing it with the ERA-Interim data (ERA-I; Dee et al. 2011).

To investigate the role of orography in shaping the zonal mean flow and stationary waves four WACCM6 simulations are performed: CTL, no mountain (NM), CTL_{smooth}, and NM_{rough}. The CTL simulation has present-day topography, while the NM simulation has all topography flattened to sea level. In addition to flattening the resolved orography in the NM experiment, we reduce all boundary condition variables associated with sub-grid-scale orographic variability to 0 (the value over the ocean), effectively switching off all parameterized responses to unresolved orography, including the turbulent orographic form drag, orographic gravity wave drag, and the nonlinear near-surface drag. The CTL_{smooth} experiment has smooth mountains, i.e., we keep the resolved orography of CTL, but use the sub-grid-scale orographic variability of NM; the NM_{rough} simulation is the opposite to CTL_{smooth}, i.e., zero resolved orography but the same sub-grid-scale orographic variability as CTL. The simulations are 20 years in length (following a 1-yr spinup period). All responses analyzed in this study are large relative to the interannual variability, and so 20 years is found to be sufficient to obtain a robust signal (not shown). Significance testing confirms that this is true even in the stratosphere, where interannual variability is relatively large. We run sensitivity experiments at 1.9° × 2.5° (hereafter ~2°) to test the sensitivity of our results to horizontal resolution. We also run sensitivity experiments using an earlier version of the model, the WACCM4, which uses different parameterizations of the unresolved orography. Our conclusions are unchanged by these changes in resolution or model version (results presented in the online supplemental material).

Orographic forcing can also influence SSTs through air–sea heat fluxes (Okajima and Xie 2007; Chang 2009); this may affect the impact of orography on diabatic heating, although historically this effect has been considered to be small (Held 1983). Additionally, changes in SSTs may alter circulation patterns and thus the winds impinging on orography; this can affect the atmospheric response to orography. We repeat some of our key simulations with the atmosphere model coupled to a slab ocean, which allows the SSTs to adjust to changes in air–sea heat fluxes; this has little impact on our conclusions. These results are not shown, but are discussed briefly in section 4. Mountains are also known to affect ocean circulation (Kitoh 2002; Sinha et al. 2012) through impacts on wind stress and freshwater fluxes (Warren 1983; Emile-Geay 2003), which can further affect surface heat fluxes. Here we focus on the dynamical atmospheric response to global mountain ranges and do not consider dynamical ocean changes.

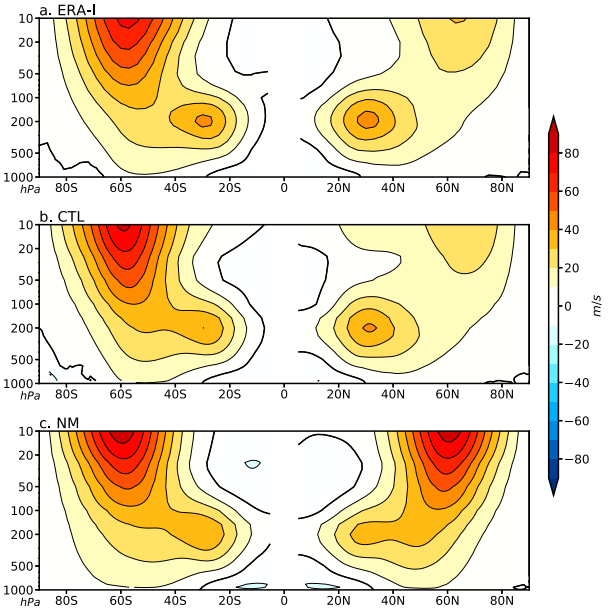

FIG. 1. Wintertime (DJF in the NH and JJA in the SH) zonal mean zonal wind $\overline{U}$ in m s^{-1}: (a) ERA-I, (b) CTL, and (c) NM. In all plots values are masked between 10°S and 10°N to emphasize the discontinuity in the plotted season at the equator.

3. Results

In section 3a we present the effects of orography on the wintertime axisymmetric flow, including a separation of the impacts of resolved orography and parameterized orographic drag, and compare the relative importance of different mechanisms. Following this, in section 3b we present the impacts of orography on wintertime stationary waves.

a. Zonal mean response to orography

Orography substantially decelerates NH wintertime zonal mean zonal wind $\overline{U}$ (overbar denotes zonal mean) throughout most of the extratropical troposphere and stratosphere. Figure 1 shows ERA-I and WACCM pole-to-pole meridional cross sections of $\overline{U}$. Winter is shown for each hemisphere, i.e., DJF in the NH and JJA in the SH. The WACCM reproduces the general structure of wintertime $\overline{U}$ in both hemispheres well (cf. Figs. 1a and 1b), including the difference in the strength of the NH and SH stratospheric jets. The NM fields (Fig. 1c) have remarkable symmetry between the NH and SH, showing that orography dominates over land–sea contrast in producing the hemispheric differences in the stratospheric winter jet (see also White et al. 2018). As implied by the comparable magnitudes

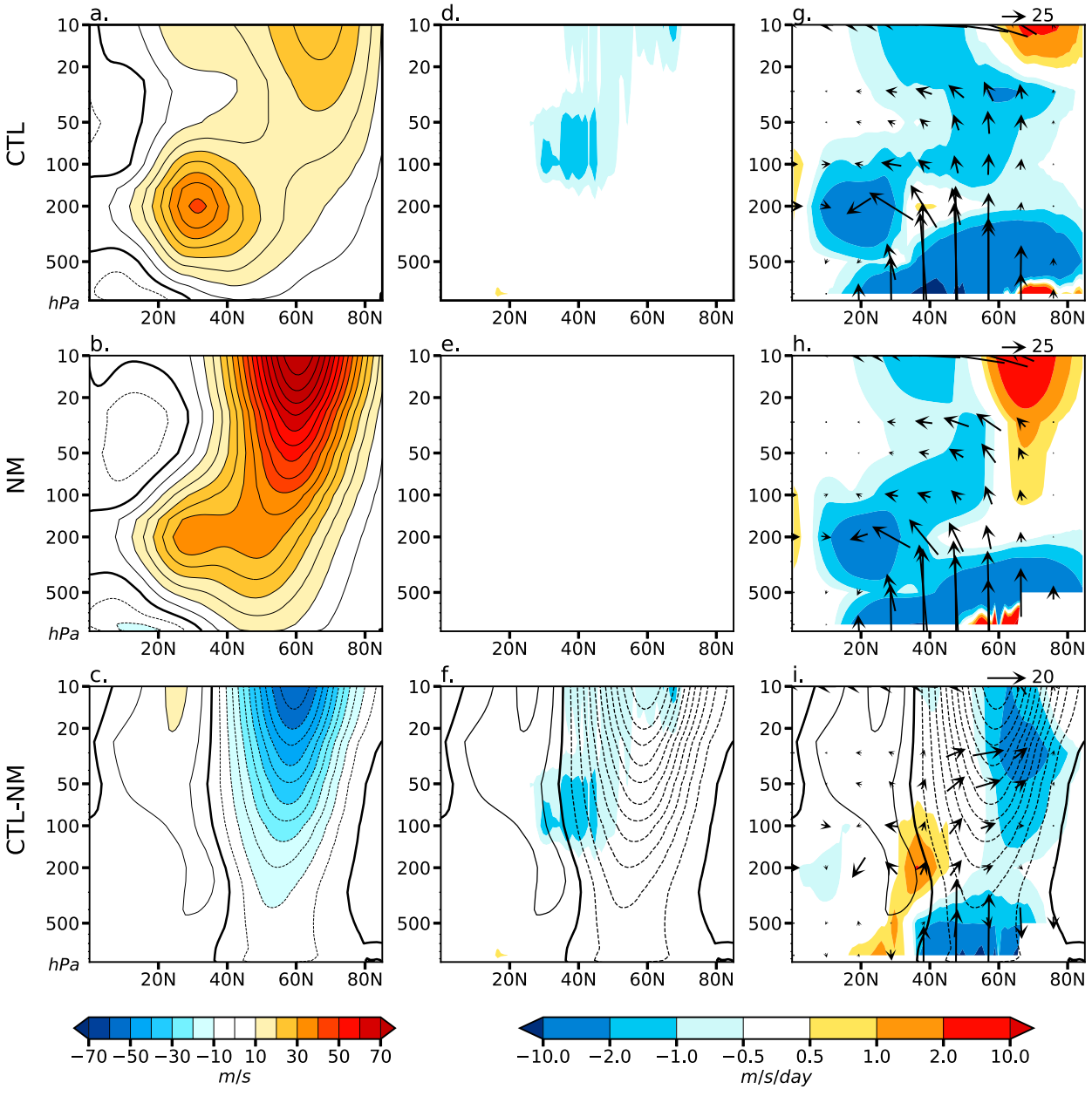

FIG. 2. (a)–(c) DJF $\overline{U}$, (d)–(f) orographic gravity wave drag, and (g)–(i) EP fluxes and their divergence for (top) CTL, (middle) NM, and (bottom) the response to orography CTL − NM. In (f) and (i), the total CTL − NM change in $\overline{U}$, repeated from (c), is shown in black contours (interval of 5 m s^{-1}, with negative dashed and zero contour bold). Note the nonlinear color scale (d)–(i). For display of the EP flux vectors (arrows) in both the troposphere and stratosphere we follow the scaling of Edmon et al. (1980) for log-pressure coordinates, and divide by the square root of 1000/pressure as in Taguchi and Hartmann (2006); the arrows thus cannot be used to estimate divergence.

of the subtropical jets (equatorward of 40°N/S) in the two hemispheres in both observations/reanalysis data and the CTL experiment (Figs. 1a,b), the impact of orography on the zonal mean subtropical jet strength is small (<10% of the CTL value); however, north of 40° N orography slows down $\overline{U}$ throughout the troposphere and stratosphere. Differences are most noticeable in the stratosphere, where the presence of orography reduces the stratospheric jet by up to 80% (i.e., to approximately 20% of the NM jet strength); near the surface $\overline{U}$ is reduced by 50%–80% poleward of 50°N (see Fig. 2 and Fig. S1 in the online supplementary material for a focus on the tropospheric change). In the SH there is little impact of topography on $\overline{U}$ outside of the polar region.

Figure 2 shows NH $\overline{U}$ (left column) in meters per second, and the forcing of $\overline{U}$ by two key components of the response to orography: parameterized orographic gravity wave drag (center column) and resolved wave forcing (right column) in meters per second per day. Parameterized low-level drag is not shown

in these figures as the forcing is not an output of WACCM; the likely impacts of this forcing are discussed further below. In Fig. 2 the CTL and NM simulations are shown in the first two rows, with the effect of orography, i.e., CTL − NM, in the bottom row. The resolved wave forcing in the right column is shown by the Eliassen–Palm (EP) wave activity fluxes (arrows) and their divergence (colors); these are calculated on daily wintertime data, i.e., for the total (transient and stationary) resolved wave activity (Eliassen and Palm 1961). The EP flux arrows are scaled (see figure caption) and thus cannot be used to estimate divergence/convergence. Convergence of EP flux signifies a weakening of the zonal mean flow by the waves (Andrews and McIntyre 1976; Edmon et al. 1980). The forcing from the gravity wave parameterization (center column) and EP flux divergence (right column) are shown on the same, nonlinear, scale. As the atmosphere has different relaxation time scales at different altitudes, one should not expect the change in $\overline{U}$ per unit forcing to be equal throughout the atmospheric column.

In the free troposphere there is little to no contribution from gravity wave drag in the CTL simulation (Fig. 2d), as expected, and a deceleration from resolved EP convergence (Fig. 2g), consistent with previous research (Edmon et al. 1980; Li et al. 2011). In the stratosphere there is generally deceleration from both orographic gravity wave forcing and resolved waves, with stronger forcing from the resolved waves (cf. Figs. 2d,g). In the NM simulation (second row), there is no orographic gravity wave drag, and the deceleration from EP flux convergence is reduced in the stratosphere. In the high-latitude stratosphere, there is divergence of EP fluxes in the NM simulation, suggesting a local wave source and acceleration of the zonal flow by wave activity; this is consistent with observations of the Southern Hemisphere (e.g., Hartmann et al. 1984; Randel and Lait 1991).

Figure 2c shows that orography greatly slows down $\overline{U}$ poleward of 40°N. This deceleration, while strongest in the stratosphere, is present throughout the troposphere to the surface. The change in $\overline{U}$ seen in this panel is repeated in black contours in Figs. 2f and 2i. In the stratosphere the CTL − NM changes in orographic gravity wave forcing (Fig. 2f) are of smaller amplitude than the changes in resolved wave forcing (Fig. 2i); however, the parameterized gravity wave drag deceleration acts slightly equatorward of the latitude of maximum deceleration (Fig. 2f), and the forcing from EP fluxes slightly poleward (Fig. 2i), suggesting both play a role in the total deceleration. Note that the increased divergence of EP fluxes around 40°N and 200 hPa likely reflects changes in wave propagation in response to the removal of the orography, not a local wave source.

Other impacts of parameterized orographic drag, including the drag from the TOFD parameterization and nonlinear processes near the surface, likely also play a significant role in the low-level $\overline{U}$ response to orography. Unfortunately these forcings are not provided as an output of the WACCM6 model and so are not included in Fig. 2 or Fig. 3. Lindvall et al. (2017) use a previous version of the CESM model and find that switching off a form drag parameterization similar to the TOFD leads to an increase of up to 2 m s^{-1} in annual mean $\overline{U}$ between 40° and 60°N. This implies that the parameterization of low-level form drag plays a significant role in the lower-tropospheric decrease in $\overline{U}$ of 5–10 m s^{-1} in response to orography (Fig. 2c). Our sensitivity studies show a slightly enhanced deceleration from parameterized orographic drag in the WACCM6 relative to the WACCM4, particularly near the surface (shown in Fig. S2). Thus the parameterized low-level drag in WACCM6 (from both the TOFD parameterization and nonlinear near-surface drag) likely has an even larger impact on the near surface winds than that seen in the Lindvall et al. (2017) study.

Resolved orographic pressure torque contributes to the resolved response to orography. This torque is estimated for the CTL simulation using the surface pressure method of Wahr and Oort (1984): summing a value proportional to $p_s \times 0.5(H_{i+1} - H_{i-1})$ over all grid boxes i along a circle of constant latitude, where p_s is surface pressure and H is surface height. This gives values in quantitative agreement with observations from Tucker (1960) and Madden and Speth (1995) for the CTL simulation. Between 40° and 70°N, where orography has the largest impact on $\overline{U}$, the resolved orographic pressure torque is found to be an order of magnitude lower than that from the resolved wave forcing shown in Figs. 2g and 2h, and thus we conclude that resolved orographic pressure torque does not play a substantial role in the total forcing of $\overline{U}$ in the free troposphere by orography.

RESOLVED OROGRAPHY VERSUS PARAMETERIZED OROGRAPHIC DRAG

We now decompose the total response to orography into that forced by the large-scale resolved orography ($\text{CTL}_{\text{smooth}}$ − NM), and that forced by parameterized orographic drag (CTL − $\text{CTL}_{\text{smooth}}$). The decomposition can be seen in Fig. 3, where the first row repeats the CTL − NM fields shown in the bottom row of Fig. 2, the middle row shows the impact of resolved orography, and the bottom row that of parameterized orographic drag. The total response to parameterized orography is a combination of the parameterized gravity wave response (Fig. 3f), parameterized low-level drag (TOFD and nonlinear drag from the orographic gravity wave scheme; not shown), as well as subsequent changes in resolved wave forcing (Fig. 3i). Parameterized orography has a much greater influence on $\overline{U}$ than resolved orography throughout the midlatitude atmospheric column, producing 60%–80% of the total weakening (cf. Figs. 3a–c). This result is remarkably robust to changing the model spatial resolution from ~1° to ~2°, with small quantitative differences in the $\overline{U}$ response to resolved and parameterized orography (see Fig. S2). Calculating the resolved orography response using CTL − NM_{rough} and the parameterized orography response using NM_{rough} − NM gives a very similar result to that seen in Fig. 3 (shown in Fig. S3): the $\overline{U}$ response is dominated by the response to parameterized orography, with resolved waves playing a significant role in this response, particularly in the stratosphere.

Parameterized orography dominates both changes in orographic gravity wave drag (as expected) as well as changes in resolved wave forcing, at least away from the surface (cf. Figs. 3d–i). Resolved orography acts as a strong source of resolved wave activity at the surface around 40°–60°N, where

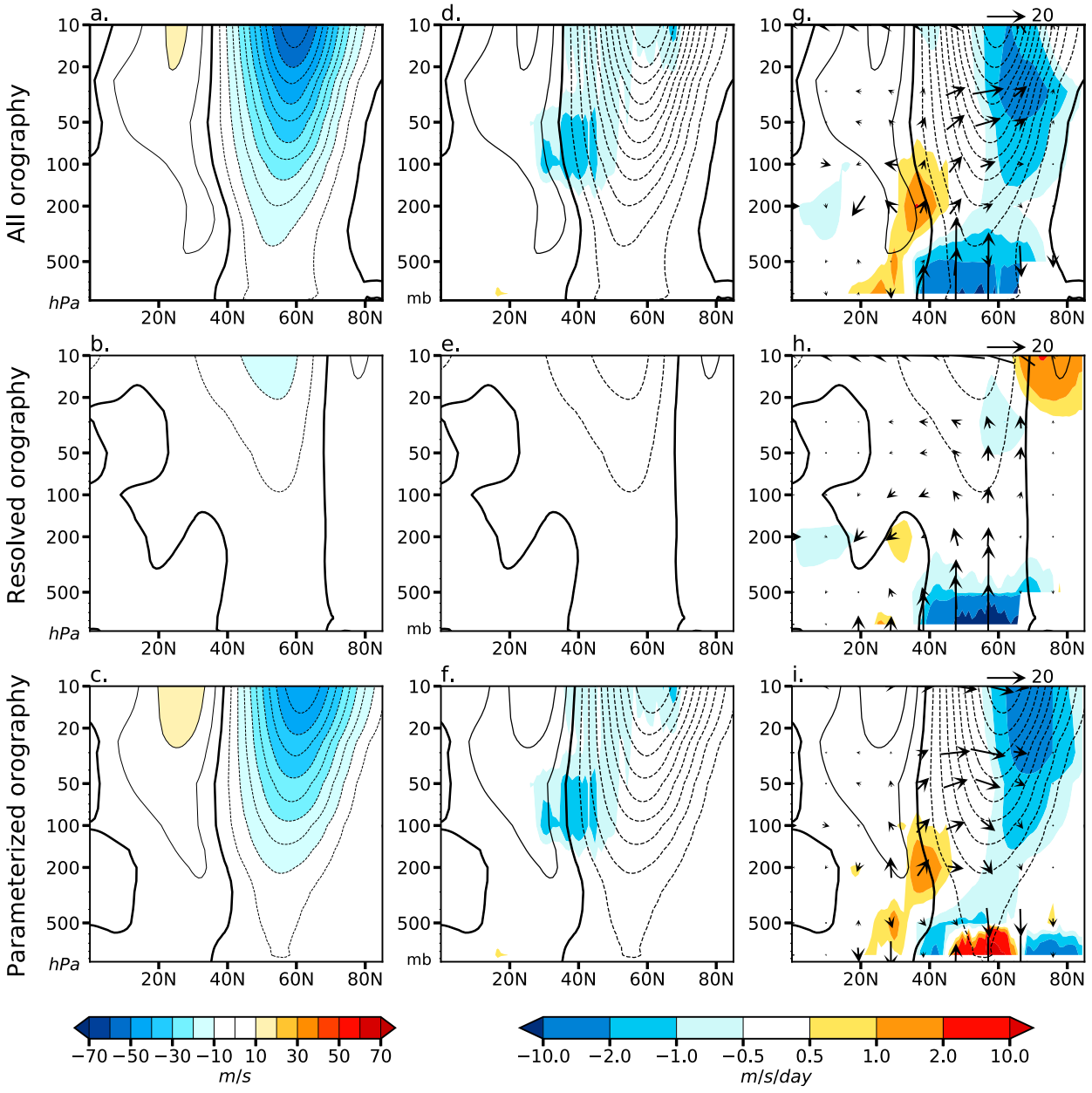

FIG. 3. As in Fig. 2, but for (top) CTL − NM (repeated from bottom row of Fig. 2), (middle) the response to resolved orography (CTL_{smooth} − NM), and (bottom) the response to parameterized orography (CTL − CTL_{smooth}).

strong surface westerlies interact with the major NH mountain ranges (White et al. 2017); this surface wave source can be seen in the upward EP flux arrows emanating from the bottom of Fig. 3h. Most of this wave activity, however, converges below 500 hPa, with relatively little able to propagate into the stratosphere to converge and decelerate stratospheric $\overline{U}$. Conversely, parameterized orography acts to weaken the stratospheric flow around 40°N through parameterized orographic gravity wave drag (Fig. 3f), with further weakening through resolved wave forcing (Fig. 3i). This resolved wave forcing occurs despite no strong surface source of resolved wave activity in response to the parameterized orography—the arrows in the lower troposphere in Fig. 3i are largely downward, suggesting a reduction of the surface wave source. The increase in resolved wave forcing in response to parameterized orography must therefore result predominantly from changes in the propagation of waves. A mechanism for how parameterized orography impacts stratospheric $\overline{U}$ through resolved wave forcing is presented and discussed in section 4.

b. *Stationary wave response to orography*

We analyze stationary waves through the climatological eddy geopotential height: $Z' = Z - \overline{Z}$. Figure 4 shows Z' at 45°N for ERA-I, the CTL and NM simulations, and the CTL − NM

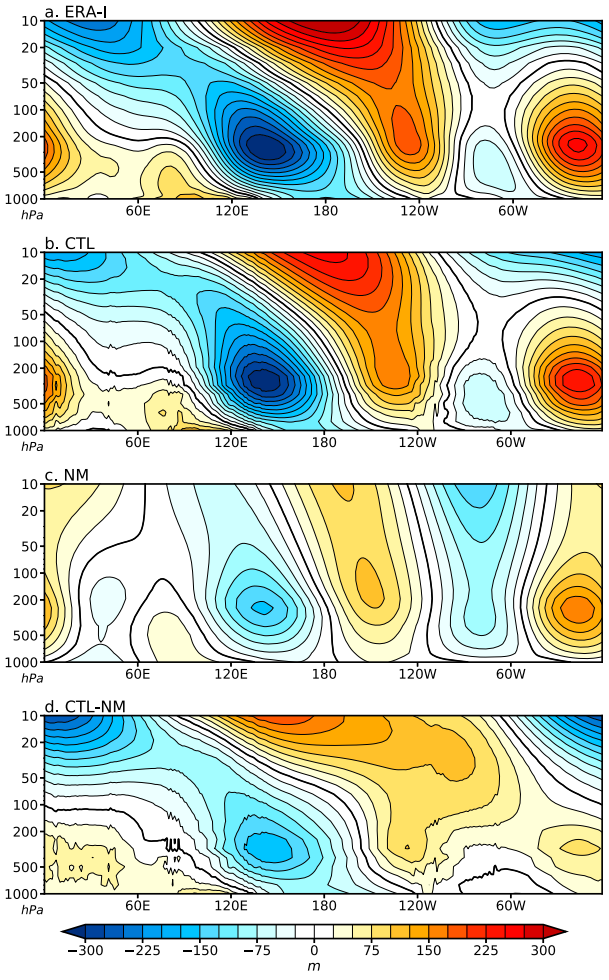

FIG. 4. DJF NH eddy geopotential height Z' (in m) at 45°N for (a) ERA-I, (b) CTL, (c) NM, and (d) CTL − NM.

difference. The CTL simulation reproduces the observed pattern from ERA-I well (cf. Figs. 4a,b). The stationary waves in the CTL and NM simulations, and thus the stationary wave response to orography (CTL − NM), is broadly similar to that found in earlier studies using climate models (e.g., Held 1983). The orography-induced stationary waves (CTL − NM) and the stationary waves from land–sea contrasts alone (NM) are generally of similar magnitude, although in the stratosphere the orographic forcing is much more important than the land–sea forcing (cf. Figs. 4c,d).

The spatial distribution of the response to all orography in Fig. 4d is broadly consistent with previous studies (e.g., Held 1983). Conversely, the spatial pattern of the NM stationary wave pattern, shown in Fig. 4c, shows some differences, including a higher wavenumber, than in some previous studies (e.g., Held 1983; Nigam et al. 1986). As will be discussed in section 4, the NM stationary wave pattern is very sensitive to small differences in tropical SSTs, and thus differences between NM simulations in different studies may be due to differences in tropical SST fields.

To study the horizontal structure of the stationary wave response to orography, Fig. 5 shows maps of Z at 1000, 300, and 30 hPa, with contours showing the full fields and colors showing the eddy component, Z'. The WACCM reproduces the ERA-I spatial pattern of stationary waves well (cf. Fig. 5 top row with the middle row). The midlatitude stationary wave pattern is much weaker in NM than in CTL throughout the troposphere and stratosphere. Near the surface, the Z' pattern in CTL is predominantly due to the presence of orography: without mountains the near-surface stationary wave has little resemblance to the CTL stationary wave (cf. Figs. 5b,c). In the upper troposphere the NM eddy field (Fig. 5f) exhibits a spatial structure similar to that of CTL (Fig. 5e), but with muted amplitude. This suggests a constructive interference between the NM and orographically forced stationary waves, noted by Held (1983), Held et al. (2002), and Chang (2009). This can also be seen in the cross section of Z' in Fig. 4, where the free troposphere response to orography (Fig. 4d) generally projects onto the NM stationary wave pattern (Fig. 4c), with a strong low centered around 150°E and highs at around 130° and 30°W. This constructive interference, which is sensitive to the tropical SSTs specified in the NM case (see section 4), helps augment the magnitude of the free troposphere stationary wave in the CTL simulation, particularly the low in the western Pacific (120°E–180°) and the high over the Atlantic and eastern Europe (60°–0°W). The NM stratospheric stationary wave is weak and has little resemblance to that in the CTL simulation (cf. Fig. 4c with Figs. 4d and 5g–i).

RESOLVED OROGRAPHY VERSUS PARAMETERIZED OROGRAPHIC DRAG

The stationary wave response is now separated into the response to resolved and parameterized orography using the $\mathrm{CTL}_{\mathrm{smooth}}$ simulation (Fig. 6). Near the surface, both resolved and parameterized orography play approximately equal roles in the total stationary wave response (cf. Figs. 6b,c). In the upper troposphere and stratosphere the response to resolved orography is slightly stronger than the response to parameterized orography (cf. Fig. 6e with Figs. 6f,h with Fig. 6i). The total response to orography is spatially much more similar to the response to resolved orography (cf. Fig. 6d with Figs. 6e,g with Fig. 6h), than to the parameterized orography (cf. Fig. 6d with Figs. 6f,g with Fig. 6i), suggesting the response to resolved orography is dominant. This conclusion holds when we use the $\mathrm{NM}_{\mathrm{rough}}$ experiment to separate resolved and parameterized orography, although the stationary wave response to parameterized orography is much stronger when resolved orography is present (i.e., CTL − $\mathrm{CTL}_{\mathrm{smooth}}$) than when resolved orography is absent (i.e., $\mathrm{NM}_{\mathrm{rough}}$ − NM).

4. Discussion

a. A proposed mechanism for the impacts of orography on stratospheric $\overline{U}$

That *parameterized* orography impacts stratospheric $\overline{U}$ predominantly through changes in *resolved* waves may provide some insights into real world troposphere–stratosphere coupling. Based on the results presented in this paper, we put forward the following mechanism for how orography influences stratospheric $\overline{U}$, illustrated in the schematic in Fig. 7. In the

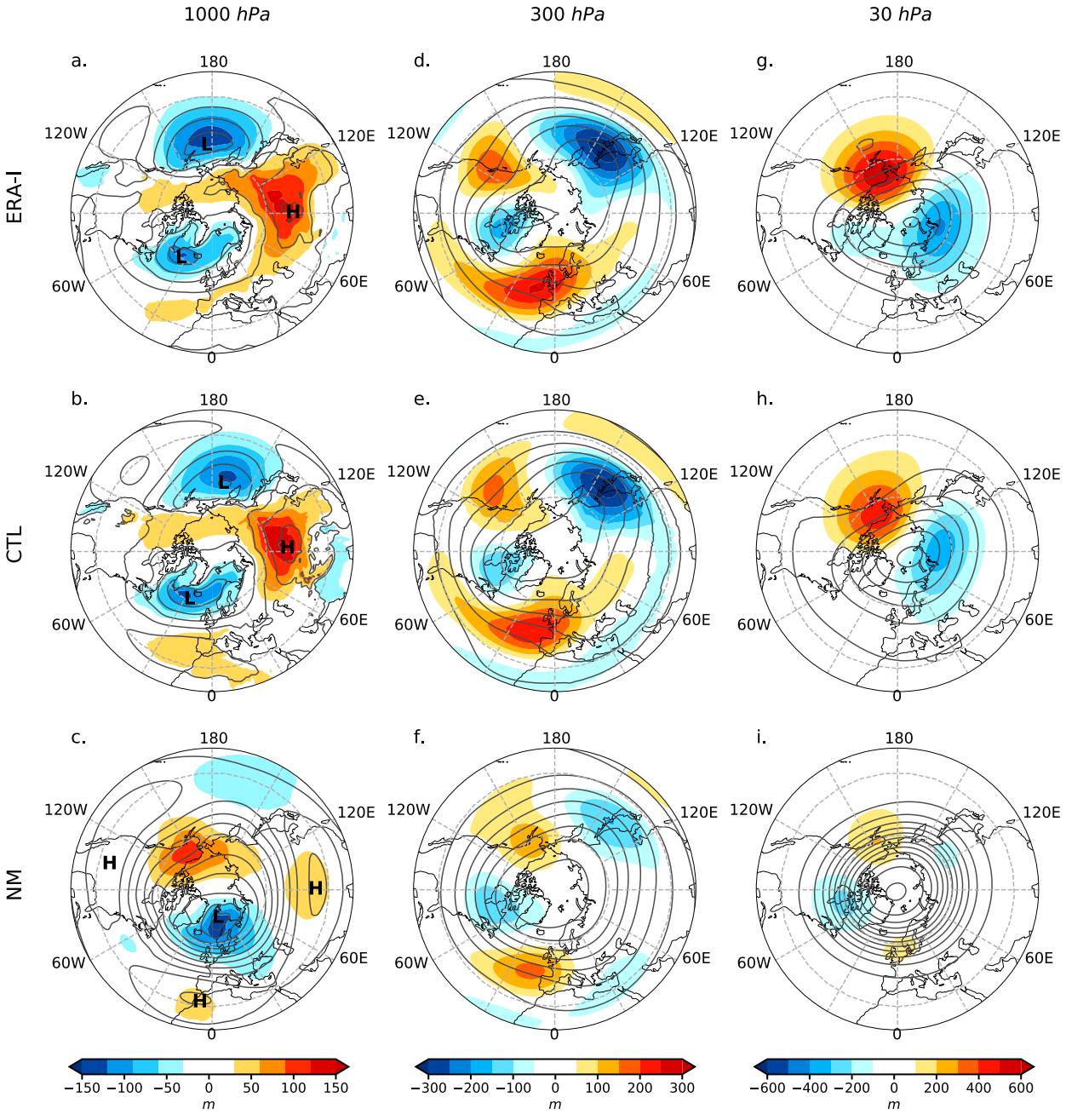

FIG. 5. DJF NH geopotential height Z (in m), full fields (contours), and eddy component Z' (colors) at (a)–(c) 1000, (d)–(f) 300, and (g)–(i) 30 hPa for (top) ERA-I, (middle) CTL, and (bottom) NM. Prominent highs and lows in the full surface fields are denoted with H and L, respectively, in (a)–(c). The contour interval for the full fields is 50, 200, and 250 m at 1000, 300, and 30 hPa, respectively.

world without orography (top left), $\overline{U}$ is strong throughout much of the extratropical troposphere and stratosphere. Adding in the parameterized orographic drag (arrow A) produces gravity waves that propagate into and break within the stratosphere, decelerating the zonal flow there (top-right panel), as well as low-level drag close to the surface. The slower stratospheric flow extends the range of wavenumbers that can propagate into the stratosphere (arrow B; Charney and Drazin 1961). Combined with the increased surface source of waves by the resolved orography, this increase in permitted wavenumbers results in increased wave dispersion into the stratosphere (black EP flux arrows in bottom-right panel); note that the upward EP fluxes into the stratosphere are close to the latitude of the gravity wave forcing. This increased vertical wave propagation, along with changes in the propagation pathways in the stratosphere (see also White et al. 2018), leads to increased EP flux convergence (colors in lower-right panel), further reducing $\overline{U}$ (arrow C) and resulting in

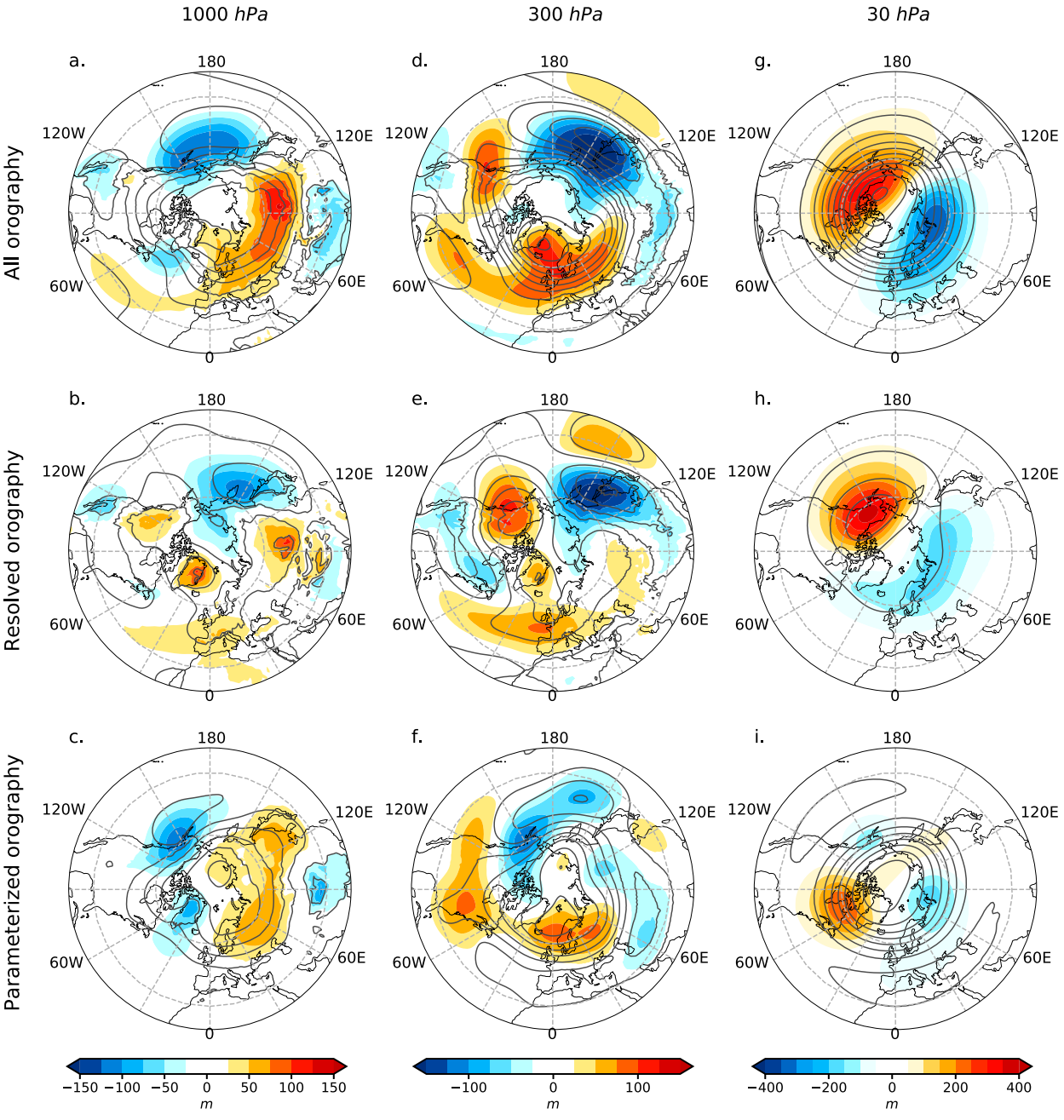

FIG. 6. As in Fig. 5, but for the (top) total orographic response (CTL − NM), (middle) resolved orography response (CTL_{smooth} − NM) and (bottom) response to parameterized orography (CTL − CTL_{smooth}). The contour interval for the full fields is 50, 50, and 200 m at 1000, 300, and 30 hPa, respectively.

the observed $\overline{U}$ (bottom-left panel). This can be considered a catalytic positive feedback in $\overline{U}$, wherein a decrease of stratospheric $\overline{U}$ due to gravity wave drag leads to changes in planetary (resolved) wave propagation such that $\overline{U}$ is further reduced. This mechanism, in which parameterized orography affects the background state in which resolved waves propagate, is consistent with the results and conclusions of Sigmond and Scinocca (2010) as well as work by Polichtchouk et al. (2018) looking at the effects of parameterized nonorographic wave drag. The proposed mechanism explains how parameterized orography can increase wave forcing of the stratospheric mean flow without an increase in the surface source of wave activity, as highlighted in section 3a.

It is notable that resolved wave convergence in the stratosphere is more impacted by the presence of *parameterized* orography than by the presence of *resolved* orography (see Fig. 3 and Fig. S3). Resolved orography acts as a surface source of

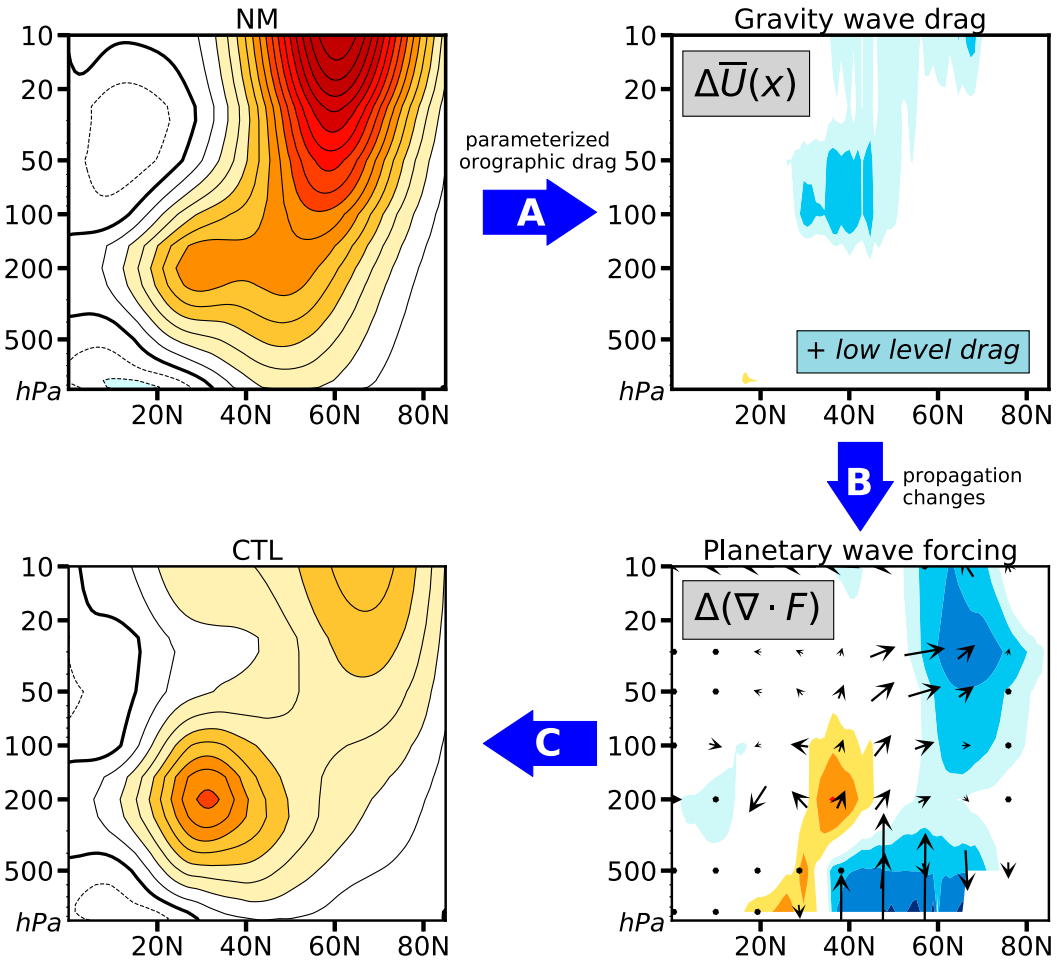

FIG. 7. Schematic showing the influence of orography on DJF NH stratospheric $\overline{U}$, starting with the NM flow and proceeding clockwise: adding in orographic roughness (arrow A) leads to a upper-stratospheric forcing of $\overline{U}$ by gravity wave drag. This reduction of $\overline{U}$ initiates the $\overline{U}$ feedback (arrow B), allowing increased propagation into and convergence within the stratosphere of resolved wave activity from all sources (thermal contrast and resolved orography). This change in resolved forcing dominates the total stratospheric change in $\overline{U}$ (arrow C; cf. the contours in Figs. 3a–c), resulting in the observed distribution of $\overline{U}$ in CTL.

resolved waves, producing a small increase of EP flux propagation into the stratosphere, which results in a small reduction of $\overline{U}$ (Fig. 3h and Fig. S3h). It seems, however, that this small decrease is insufficient, or at the wrong latitude, to trigger the positive feedback that leads to a strong stratospheric response. This is suggestive of a threshold behavior, similar to that seen in sudden stratospheric warmings (e.g., Butler et al. 2017; White et al. 2018; Nakamura et al. 2020), during which the stratospheric polar vortex rapidly breaks down over the course of a few days, and the high-latitude stratospheric zonal winds reverse direction. The threshold behavior also suggests that the response to orography may be sensitive to the latitude at which the parameterized gravity waves break, which may be dependent on model resolution and/or the parameterization scheme. The sensitivity experiments presented in Fig. S2, however, find that our conclusions are robust to at least some differences in model resolution and version. The resolved wave forcing of stratospheric $\overline{U}$ in response to parameterized orography is almost as strong in the absence of resolved orography (i.e., $\mathrm{NM}_{\mathrm{rough}}$ − NM, Fig S3i) as it is in the presence of resolved orography (i.e., CTL − $\mathrm{CTL}_{\mathrm{smooth}}$, Fig. 3i), suggesting that the additional waves created by the resolved orography provide only a small contribution to the total stratospheric response.

b. *Impact of SSTs*

All of the simulations presented in this paper use fixed, present-day, SSTs. We investigated the sensitivity of our results to this choice of lower boundary condition by running simulations with the atmosphere model coupled to a slab-ocean model, thus allowing the SSTs to change in response to changing surface heat fluxes, but not considering ocean circulation changes. Through a series of experiments in which we limit changes in SST to the tropics and/or extratropics, we find that the extratropical SST changes caused by the presence of orography have little impact on the results and conclusions

presented. Both the strength and the spatial pattern of stationary waves in the NM simulations, however, are remarkably sensitive to relatively small (~1 K) changes in the tropical SSTs. This is consistent with previous work finding a strong sensitivity of midlatitude circulation and stationary waves to tropical SSTs (e.g., Yin and Battisti 2001; Held et al. 2002; Inatsu et al. 2002), although our results suggest that in the real world orography reduces the sensitivity somewhat. Tropical SST changes induced by substantial shifts in ocean circulation due to the presence/absence of orography could affect our conclusions.

c. *The importance of the location and orientation of orography*

To further understand the results presented in this study, and test how sensitive the atmospheric response to orography is to the relative distribution and orientation of orography and land boundaries on present-day Earth, we also run simulations at ~2° horizontal resolution with a backward-rotating Earth, CTL_{BW} and NM_{BW}. We set Earth's angular rotation rate $\omega_{BW} = -1.0\omega$. These simulations have the same imposed SSTs as the standard simulations, including the effects of western boundary currents, thereby ignoring changes in air–sea fluxes and ocean circulation from the reversed rotation direction. Sensitivity experiments using slab oceans with zonal mean q fluxes (i.e., assuming no longitudinal dependence of oceanic heat transport) in both forward and backward simulations find that our conclusions are insensitive to this choice of SSTs. In these retrograde-rotating Earth simulations, there is easterly flow in the midlatitudes, and thus the location of the most prominent orography relative to the boundaries where air flows from ocean to land is changed substantially from the real world, as well as substantial changes in the orientation of mountain ranges relative to the impinging winds. The results are summarized in the supplementary material; see Figs. S4 and S5. We use these experiments to highlight the importance of the orography–land configuration on the effect of orography on the atmospheric circulation. For a study of the climate of a retrograde-rotating Earth, including a dynamic coupled ocean, see Mikolajewicz et al. (2018).

The strength of $\overline{U}$ in the NM simulations is very similar in the forward and backward simulations (cf. Fig. 2b with Fig. S4b); however, in the backward-rotating Earth the presence of orography has only 50%–70% of the impact on $\overline{U}$ in the free troposphere and stratosphere relative to forwards Earth (cf. Fig. 2c with Fig. S4c). In the presence of orography, the stationary waves are substantially weaker on a backward-rotating Earth, particularly in the free troposphere (cf. Figs. S5a and S5c) and stratosphere. Conversely, in the NM simulations the stationary waves are only slightly weaker on backward-rotating Earth (cf. Figs. S5b and S5d). Much of the difference in stationary wave strength between CTL and CTL_{BW} is thus due to differences in the strength of the response to orography, which is much weaker on backward-rotating Earth. This weaker impact of orography on the stationary waves in backward Earth is consistent with a weaker change in resolved wave forcing (cf. Fig. 2i with Fig. S4i), and thus smaller changes in $\overline{U}$ in the free troposphere and stratosphere. This is consistent with the mechanism presented in Fig. 7.

TABLE 1. Maximum annual mean NH atmospheric meridional heat transport (AHT) in various simulations. Values in parentheses show differences from the CTL simulation. Standard error of the mean shown for the CTL is based on assuming independence of each year in the 20-yr simulation. Conclusions are very similar for the SH.

Expt	Max AHT (PW)
CTL	4.65 ± 0.01
NM	4.57 (−0.08)
CTL_{BW}	4.47 (−0.18)
NM_{BW}	4.70 (+0.05)

d. *Stationary waves and meridional heat transport*

Last, we consider the impact of the substantially different stationary wave amplitudes on the atmospheric meridional heat transport in these different climates. Previous work has found that, for any given model, the maximum meridional heat transport is remarkably constant across a range of different climates, despite large differences in the partitioning of energy transport: e.g., stationary versus transient and/or moisture versus sensible heat transport (Donohoe and Battisti 2012; Donohoe et al. 2020). These studies looked at realistic climates ranging from the Last Glacial Maximum to CO_2 forcing experiments. Our NM simulations, particularly NM_{BW}, provide a stronger test of the invariance in maximum meridional heat transport. Table 1 summarizes the maximum meridional atmospheric heat transport (AHT) calculated using the difference between top of atmosphere radiative fluxes and surface heat fluxes (as in Donohoe et al. 2020). Despite markedly different climates and stationary wave strengths, the maximum AHT varies by less than 4%. Any changes in absorbed solar radiation from cloud or surface albedo changes must therefore be almost completely compensated by changes in outgoing longwave radiation. Interestingly, simply changing the version of the same model (WACCM4 and WACCM6) gives differences of ~12% for the CTL simulation, a much larger difference than removing mountains and rotating Earth backward in the same model. These experiments provide further evidence of the remarkable consistency of maximum AHT, for a given model, to a vast range of climates.

5. Summary

The impact of global orography on the climatological wintertime circulation is examined with the WACCM6 at 1° horizontal resolution, revisiting the seminal work of the 1980s and 1990s with a state-of-the-art climate model. We also quantify the relative contributions from resolved and parameterized orography. Through comparisons of simulations with and without orography, we find the following:

Orography substantially slows $\overline{U}$ poleward of 40°N. Throughout the NH extratropical troposphere and stratosphere orography reduces $\overline{U}$ by 50%–80%, such that, without orography, the NH wintertime stratospheric zonal mean flow is comparable in strength to that of the observed SH winter jet. In this model parameterized orographic drag accounts for more than 2/3 of

the total slowdown of $\overline{U}$ in response to orography. The parameterization of unresolved orography has been highlighted in recent literature as important for both weather forecasting models and climate models (e.g., Sandu et al. 2019); our results further emphasize the importance of these parameterizations, including the influence on resolved wave propagation. Previous estimates suggested a much weaker role of orography on $\overline{U}$ (e.g., Manabe and Terpstra 1974); this discrepancy likely stems from the importance of the impacts of unresolved orography, which are better represented in the more sophisticated parameterizations of today's models.

Orography contributes at least as much as land–sea contrast and SSTs to the NH stationary waves. The observed features of the stationary waves in the lower troposphere—including the Aleutian low and Siberian high—are weak or absent in the absence of orography (Fig. 5, left column). In the free troposphere, the stationary waves attributable to land–sea contrast and orography are of approximately equal amplitude. In the stratosphere, stationary waves are predominantly driven by orography. These results are broadly consistent with previous work, but suggest a more important role for orography than the most recent estimates (e.g., Ting et al. 2001; Held et al. 2002; Chang 2009). The increased importance of orography in our study relative to previous work may be due to the role of parameterized orographic drag in forcing stationary waves (Fig. 6, bottom row), or due to differences in tropical SSTs, which we find to have a strong influence on the NM stationary waves.

Stationary waves depend on the positioning of orography relative to the land–sea boundaries. By repeating our CTL and no-mountain (NM) simulations with Earth rotating backward, we find that the orographic impact on both $\overline{U}$ and stationary wave is weaker on a backward-rotating Earth. The strength of the stationary waves in the present climate is thus dependent on the position and orientation of large-scale mountain regions relative to the coastlines (see also Brayshaw et al. 2009). This result has potential implications for the efficacy of using idealized models to assess the impact of orography on climate, and for understanding how paleoclimates differed from today.

Amalgamating these results, along with the sensitivity of the NM stationary waves to tropical SSTs discussed in the previous section, leads to the conclusion that producing a precise estimate of the role of orography in the forcing of the observed stationary waves is a formidable, and potentially impossible, task. The substantial impact of orography on the zonal mean flow means that stationary wave models, in which zonal mean flow is prescribed, cannot provide a full, or potentially even a meaningful, answer to this particular problem. By ignoring the impact of orography on the zonal flow $\overline{U}$, stationary wave models are inflating the relative importance of land–sea contrast. In addition, Garfinkel et al. (2020) highlight strong nonlinearities involving the different contributions to the stationary waves. Complex GCMs, such as the one used in this study, include the impact of orography on $\overline{U}$, and many of the nonlinear interactions; however, fully quantifying the impact of orography would require relatively precise knowledge of the tropical SST distribution in a world without orography, a daunting challenge given the potential role of orography on ocean circulation (e.g., Sinha et al. 2012; Baldwin et al. 2021).

To conclude, orography plays a substantial role in producing the observed stationary waves, more so than most recent work suggests, perhaps due to the inclusion of relatively sophisticated parameterizations of sub-grid-scale orographic drag in the model used in this study. Orography also has considerable impact on the zonal mean zonal wind, explaining almost all of the difference in strength between the SH and NH zonal mean zonal wind throughout the free troposphere and stratosphere. The impact of orography on the stratosphere is dominated by the parameterized effects of unresolved orographic drag, although this manifests through a catalytic positive feedback mechanism that involves resolved processes. This study also highlights the important role of parameterized orographic drag in both stationary waves and troposphere–stratosphere coupling; insights gained by this study may be relevant for better understanding tropospheric–stratospheric connections, such as those associated with the quasi-biennial oscillation (QBO) or sudden stratospheric warmings.

Acknowledgments. RHW acknowledges support from the Natural Sciences and Engineering Research Council of Canada (NSERC) (RGPIN-2020-05783), the European Union's Horizon 2020 research and innovation programme under the Marie Skłodowska-Curie Grant Agreement 797961, from the National Science Foundation Grant AGS-1665247, and from the Tamaki Foundation. DSB was supported by the Tamaki Foundation. Simulations were performed at the Department of Atmospheric Sciences at the University of Washington, and on the NCAR's Cheyenne computer under Grant UWAS0064. The code to produce the figures shown in this paper can be found on RHW's github account (rhwhite): https://github.com/rhwhite/SupportingInformation/blob/main/JASStationaryWaves2021.ipynb. Climatological output data from the simulations can be found here: https://doi.org/10.5683/SP2/NTEUHF; for daily data please contact the authors.

REFERENCES

Andrews, D. G., and M. E. McIntyre, 1976: Planetary waves in horizontal and vertical shear: The generalized Eliassen-Palm relation and the mean zonal acceleration. *J. Atmos. Sci.*, **33**, 2031–2048, https://doi.org/10.1175/1520-0469(1976)033<2031:PWIHAV>2.0.CO;2.

Baldwin, J., A. Atwood, G. Vecchi, and D. Battisti, 2021: Outsize influence of Central American orography on global climate. *AGU Adv.*, in press.

Beljaars, A. C. M., A. R. Brown, and N. Wood, 2004: A new parametrization of turbulent orographic form drag. *Quart. J. Roy. Meteor. Soc.*, **130**, 1327–1347, https://doi.org/10.1256/qj.03.73.

Boer, G. J., N. A. McFarlane, R. Laprise, J. D. Henderson, and J.-P. Blanchet, 1984: The Canadian Climate Centre spectral atmospheric general circulation model. *Atmos.–Ocean*, **22**, 397–429, https://doi.org/10.1080/07055900.1984.9649208.

Bolin, B., 1950: On the influence of the Earth's orography on the general character of the westerlies. *Tellus*, **2**, 184–195, https://doi.org/10.3402/tellusa.v2i3.8547.

Brayshaw, D. J., B. Hoskins, and M. Blackburn, 2008: The storm-track response to idealized SST perturbations in an aqua-planet GCM. *J. Atmos. Sci.*, **65**, 2842–2860, https://doi.org/10.1175/2008JAS2657.1.

——, ——, and ——, 2009: The basic ingredients of the North Atlantic storm track. Part I: Land–sea contrast and orography. *J. Atmos. Sci.*, **66**, 2539–2558, https://doi.org/10.1175/2009JAS3078.1.

Broccoli, A. J., and S. Manabe, 1992: The effects of orography on midlatitude Northern Hemisphere dry climates. *J. Climate*, **5**, 1181–1201, https://doi.org/10.1175/1520-0442(1992)005<1181:TEOOOM>2.0.CO;2.

Butler, A. H., J. P. Sjoberg, D. J. Seidel, and K. H. Rosenlof, 2017: A sudden stratospheric warming compendium. *Earth Syst. Sci. Data*, **9**, 63–76, https://doi.org/10.5194/essd-9-63-2017.

Chang, E. K. M., 2009: Diabatic and orographic forcing of northern winter stationary waves and storm tracks. *J. Climate*, **22**, 670–688, https://doi.org/10.1175/2008JCLI2403.1.

Charney, J. G., and A. Eliassen, 1949: A numerical method for predicting the perturbations of the middle latitude westerlies. *Tellus*, **1** (2), 38–54, https://doi.org/10.3402/tellusa.v1i2.8500.

——, and P. G. Drazin, 1961: Propagation of planetary-scale disturbances from the lower into the upper atmosphere. *J. Geophys. Res.*, **66**, 83–109, https://doi.org/10.1029/JZ066i001p00083.

Chen, S.-C., and K. E. Trenberth, 1988a: Forced planetary waves in the Northern Hemisphere winter: Wave-coupled orographic and thermal forcings. *J. Atmos. Sci.*, **45**, 682–704, https://doi.org/10.1175/1520-0469(1988)045<0682:FPWITN>2.0.CO;2.

——, and ——, 1988b: Orographically forced planetary waves in the Northern Hemisphere winter: Steady state model with wave-coupled lower boundary formulation. *J. Atmos. Sci.*, **45**, 657–681, https://doi.org/10.1175/1520-0469(1988)045<0657:OFPWIT>2.0.CO;2.

Dee, D. P., and Coauthors, 2011: The ERA-Interim reanalysis: Configuration and performance of the data assimilation system. *Quart. J. Roy. Meteor. Soc.*, **137**, 553–597, https://doi.org/10.1002/qj.828.

Donohoe, A., and D. S. Battisti, 2012: What determines meridional heat transport in climate models? *J. Climate*, **25**, 3832–3850, https://doi.org/10.1175/JCLI-D-11-00257.1.

——, K. C. Armour, G. H. Roe, D. S. Battisti, and L. Hahn, 2020: The partitioning of meridional heat transport from the Last Glacial Maximum to CO_2 quadrupling in coupled climate models. *J. Climate*, **33**, 4141–4165, https://doi.org/10.1175/JCLI-D-19-0797.1.

Edmon, H. J., B. J. Hoskins, and M. E. McIntyre, 1980: Eliassen-Palm cross sections for the troposphere. *J. Atmos. Sci.*, **37**, 2600–2616, https://doi.org/10.1175/1520-0469(1980)037<2600:EPCSFT>2.0.CO;2.

Eliassen, A., and E. Palm, 1961: On the transfer of energy in stationary mountain waves. *Geofys. Publ.*, **22**, 1–23.

Emile-Geay, J., 2003: Warren revisited: Atmospheric freshwater fluxes and "Why is no deep water formed in the North Pacific." *J. Geophys. Res.*, **108**, 3178, https://doi.org/10.1029/2001JC001058.

Garcia, R. R., D. R. Marsh, D. E. Kinnison, B. A. Boville, and F. Sassi, 2007: Simulation of secular trends in the middle atmosphere, 1950–2003. *J. Geophys. Res.*, **112**, D09301, https://doi.org/10.1029/2006JD007485.

——, A. K. Smith, D. E. Kinnison, Á. Cámara, and D. J. Murphy, 2017: Modification of the gravity wave parameterization in the Whole Atmosphere Community Climate Model: Motivation and results. *J. Atmos. Sci.*, **74**, 275–291, https://doi.org/10.1175/JAS-D-16-0104.1.

Garfinkel, C. I., I. White, E. P. Gerber, M. Jucker, and M. Erez, 2020: The building blocks of Northern Hemisphere wintertime stationary waves. *J. Climate*, **33**, 5611–5633, https://doi.org/10.1175/JCLI-D-19-0181.1.

Gettelman, A., and Coauthors, 2019: The Whole Atmosphere Community Climate Model version 6 (WACCM6). *J. Geophys. Res. Atmos.*, **124**, 12 380–12 403, https://doi.org/10.1029/2019JD030943.

Hartmann, D. L., C. R. Mechoso, and K. Yamazaki, 1984: Observations of wave–mean flow interaction in the Southern Hemisphere. *J. Atmos. Sci.*, **41**, 351–362, https://doi.org/10.1175/1520-0469(1984)041<0351:OOWMFI>2.0.CO;2.

Held, I. M., 1983: Stationary and quasi-stationary eddies in the extratropical troposphere: Theory. *Large-Scale Dynamical Processes in the Atmosphere*, B. J. Hoskins and R. P. Pearce, Eds., Academic Press, 127–167.

——, and M. Ting, 1990: Orographic versus thermal forcing of stationary waves: The importance of the mean low-level wind. *J. Atmos. Sci.*, **47**, 495–500, https://doi.org/10.1175/1520-0469(1990)047<0495:OVTFOS>2.0.CO;2.

——, ——, and H. Wang, 2002: Northern winter stationary waves: Theory and modeling. *J. Climate*, **15**, 2125–2144, https://doi.org/10.1175/1520-0442(2002)015<2125:NWSWTA>2.0.CO;2.

Hoskins, B. J., and D. J. Karoly, 1981: The steady linear response of a spherical atmosphere to thermal and orographic forcing. *J. Atmos. Sci.*, **38**, 1179–1196, https://doi.org/10.1175/1520-0469(1981)038<1179:TSLROA>2.0.CO;2.

Hurrell, J. W., J. J. Hack, D. Shea, J. M. Caron, and J. Rosinski, 2008: A new sea surface temperature and sea ice boundary dataset for the Community Atmosphere Model. *J. Climate*, **21**, 5145–5153, https://doi.org/10.1175/2008JCLI2292.1.

Inatsu, M., H. Mukougawa, and S.-P. Xie, 2002: Stationary eddy response to surface boundary forcing: Idealized GCM experiments. *J. Atmos. Sci.*, **59**, 1898–1915, https://doi.org/10.1175/1520-0469(2002)059<1898:SERTSB>2.0.CO;2.

Kitoh, A., 2002: Effects of large-scale mountains on surface climate—A coupled ocean-atmosphere general circulation model study. *J. Meteor. Soc. Japan*, **80**, 1165–1181, https://doi.org/10.2151/jmsj.80.1165.

Li, Q., H.-F. Graf, and X. Cui, 2011: The role of stationary and transient planetary waves in the maintenance of stratospheric polar vortex regimes in Northern Hemisphere winter. *Adv. Atmos. Sci.*, **28**, 187–194, https://doi.org/10.1007/s00376-010-9163-7.

Lindvall, J., G. Svensson, and R. Caballero, 2017: The impact of changes in parameterizations of surface drag and vertical diffusion on the large-scale circulation in the Community Atmosphere Model (CAM5). *Climate Dyn.*, **48**, 3741–3758, https://doi.org/10.1007/s00382-016-3299-9.

Madden, R. A., and P. Speth, 1995: Estimates of atmospheric angular momentum, friction, and mountain torques during 1987–1988. *J. Atmos. Sci.*, **52**, 3681–3694, https://doi.org/10.1175/1520-0469(1995)052<3681:EOAAMF>2.0.CO;2.

Manabe, S., and T. B. Terpstra, 1974: The effects of mountains on the general circulation of the atmosphere as identified by numerical experiments. *J. Atmos. Sci.*, **31**, 3–42, https://doi.org/10.1175/1520-0469(1974)031<0003:TEOMOT>2.0.CO;2.

Marsh, D. R., M. J. Mills, D. E. Kinnison, J.-F. Lamarque, N. Calvo, and L. M. Polvani, 2013: Climate change from 1850 to 2005 simulated in CESM1(WACCM). *J. Climate*, **26**, 7372–7391, https://doi.org/10.1175/JCLI-D-12-00558.1.

McFarlane, N. A., 1987: The effect of orographically excited gravity wave drag on the general circulation of the lower stratosphere and troposphere. *J. Atmos. Sci.*, **44**, 1775–1800, https://doi.org/10.1175/1520-0469(1987)044<1775:TEOOEG>2.0.CO;2.

Mikolajewicz, U., and Coauthors, 2018: The climate of a retrograde rotating Earth. *Earth Syst. Dyn.*, **9**, 1191–1215, https://doi.org/10.5194/esd-9-1191-2018.

Miller, M. J., T. N. Palmer, and R. Swinbank, 1989: Parametrization and influence of subgridscale orography in general circulation and numerical weather prediction models. *Meteor. Atmos. Phys.*, **40**, 84–109, https://doi.org/10.1007/BF01027469.

Nakamura, N., J. Falk, and S. W. Lubis, 2020: Why are stratospheric sudden warmings sudden (and intermittent)? *J. Atmos. Sci.*, **77**, 943–964, https://doi.org/10.1175/JAS-D-19-0249.1.

Nigam, S., I. M. Held, and S. W. Lyons, 1986: Linear simulation of the stationary eddies in a general circulation model. Part I: The no-mountain model. *J. Atmos. Sci.*, **43**, 2944–2961, https://doi.org/10.1175/1520-0469(1986)043<2944:LSOTSE>2.0.CO;2.

——, ——, and ——, 1988: Linear simulation of the stationary eddies in a GCM. Part II: The ''mountain'' model. *J. Atmos. Sci.*, **45**, 1433–1452, https://doi.org/10.1175/1520-0469(1988)045<1433:LSOTSE>2.0.CO;2.

Okajima, H., and S.-P. Xie, 2007: Orographic effects on the northwestern Pacific monsoon: Role of air-sea interaction. *Geophys. Res. Lett.*, **34**, L21708, https://doi.org/10.1029/2007GL032206.

Palmer, T. N., G. J. Shutts, and R. Swinbank, 1986: Alleviation of a systematic westerly bias in general circulation and numerical weather prediction models through an orographic gravity wave drag parametrization. *Quart. J. Roy. Meteor. Soc.*, **112**, 1001–1039, https://doi.org/10.1002/qj.49711247406.

Pithan, F., T. G. Shepherd, G. Zappa, and I. Sandu, 2016: Climate model biases in jet streams, blocking and storm tracks resulting from missing orographic drag. *Geophys. Res. Lett.*, **43**, 7231–7240, https://doi.org/10.1002/2016GL069551.

Polichtchouk, I., T. G. Shepherd, and N. J. Byrne, 2018: Impact of parametrized nonorographic gravity wave drag on stratosphere-troposphere coupling in the Northern and Southern Hemispheres. *Geophys. Res. Lett.*, **45**, 8612–8618, https://doi.org/10.1029/2018GL078981.

Randel, W. J., and L. R. Lait, 1991: Dynamics of the 4-day wave in the Southern Hemisphere polar stratosphere. *J. Atmos. Sci.*, **48**, 2496–2508, https://doi.org/10.1175/1520-0469(1991)048<2496:DOTDWI>2.0.CO;2.

Richter, J. H., F. Sassi, and R. R. Garcia, 2010: Toward a physically based gravity wave source parameterization in a general circulation model. *J. Atmos. Sci.*, **67**, 136–156, https://doi.org/10.1175/2009JAS3112.1.

Ringler, T. D., and K. H. Cook, 1995: Orographically induced stationary waves: Dependence on latitude. *J. Atmos. Sci.*, **52**, 2548–2560, https://doi.org/10.1175/1520-0469(1995)052<2548:OISWDO>2.0.CO;2.

Sandu, I., P. Bechtold, A. Beljaars, A. Bozzo, F. Pithan, T. G. Shepherd, and A. Zadra, 2016: Impacts of parameterized orographic drag on the Northern Hemisphere winter circulation. *J. Adv. Model. Earth Syst.*, **8**, 196–211, https://doi.org/10.1002/2015MS000564.

——, and Coauthors, 2019: Impacts of orography on large-scale atmospheric circulation. *npj Climate Atmos. Sci.*, **2**, 10, https://doi.org/10.1038/s41612-019-0065-9.

Scinocca, J. F., and N. A. McFarlane, 2000: The parametrization of drag induced by stratified flow over anisotropic orography. *Quart. J. Roy. Meteor. Soc.*, **126**, 2353–2393, https://doi.org/10.1002/qj.49712656802.

Seager, R., D. S. Battisti, J. Yin, N. Gordon, N. Naik, A. C. Clement, and M. A. Cane, 2002: Is the Gulf Stream responsible for Europe's mild winters? *Quart. J. Roy. Meteor. Soc.*, **128**, 2563–2586, https://doi.org/10.1256/qj.01.128.

Shaw, T. A., M. Sigmond, T. G. Shepherd, and J. F. Scinocca, 2009: Sensitivity of simulated climate to conservation of momentum in gravity wave drag parameterization. *J. Climate*, **22**, 2726–2742, https://doi.org/10.1175/2009JCLI2688.1.

Sigmond, M., and J. F. Scinocca, 2010: The influence of the basic state on the Northern Hemisphere circulation response to climate change. *J. Climate*, **23**, 1434–1446, https://doi.org/10.1175/2009JCLI3167.1.

Sinha, B., A. T. Blaker, J. J.-M. Hirschi, S. Bonham, M. Brand, S. Josey, R. S. Smith, and J. Marotzke, 2012: Mountain ranges favour vigorous Atlantic meridional overturning. *Geophys. Res. Lett.*, **39**, L02705, https://doi.org/10.1029/2011GL050485.

Smagorinsky, J., 1953: The dynamical influence of large-scale heat sources and sinks on the quasi-stationary mean motions of the atmosphere. *Quart. J. Roy. Meteor. Soc.*, **79**, 342–366, https://doi.org/10.1002/QJ.49707934103.

Taguchi, M., and D. L. Hartmann, 2006: Increased occurrence of stratospheric sudden warmings during El Niño as simulated by WACCM. *J. Climate*, **19**, 324–332, https://doi.org/10.1175/JCLI3655.1.

Ting, M., H. Wang, and L. Yu, 2001: Nonlinear stationary wave maintenance and seasonal cycle in the GFDL R30 GCM. *J. Atmos. Sci.*, **58**, 2331–2354, https://doi.org/10.1175/1520-0469(2001)058<2331:NSWMAS>2.0.CO;2.

Tucker, G. B., 1960: The atmospheric budget of angular momentum. *Tellus*, **12**, 134–144, https://doi.org/10.3402/tellusa.v12i2.9385.

Valdes, P. J., and B. J. Hoskins, 1989: Linear stationary wave simulations of the time-mean climatological flow. *J. Atmos. Sci.*, **46**, 2509–2527, https://doi.org/10.1175/1520-0469(1989)046<2509:LSWSOT>2.0.CO;2.

——, and ——, 1991: Nonlinear orographically forced planetary waves. *J. Atmos. Sci.*, **48**, 2089–2106, https://doi.org/10.1175/1520-0469(1991)048<2089:NOFPW>2.0.CO;2.

van Niekerk, A., J. F. Scinocca, and T. G. Shepherd, 2017: The modulation of stationary waves, and their response to climate change, by parameterized orographic drag. *J. Atmos. Sci.*, **74**, 2557–2574, https://doi.org/10.1175/JAS-D-17-0085.1.

——, I. Sandu, and S. B. Vosper, 2018: The circulation response to resolved versus parametrized orographic drag over complex mountain terrains. *J. Adv. Model. Earth Syst.*, **10**, 2527–2547, https://doi.org/10.1029/2018MS001417.

Wahr, J. M., and A. H. Oort, 1984: Friction- and mountain-torque estimates from global atmospheric data. *J. Atmos. Sci.*, **41**, 190–204, https://doi.org/10.1175/1520-0469(1984)041<0190:FAMTEF>2.0.CO;2.

Wallace, J. M., S. Tibaldi, and A. J. Simmons, 1983: Reduction of systematic forecast errors in the ECMWF model through the introduction of an envelope orography. *Quart. J. Roy. Meteor. Soc.*, **109**, 683–717, https://doi.org/10.1002/qj.49710946202.

Warren, B. A., 1983: Why is no deep water formed in the North Pacific? *J. Mar. Res.*, **41**, 327–347, https://doi.org/10.1357/002224083788520207.

Waugh, D. W., and L. M. Polvani, 2010: Stratospheric polar vortices. *The Stratosphere: Dynamics, Transport, and Chemistry*, L. M. Polvani, A. H. Sobel, and D. W. Waugh, Eds., Amer. Geophys. Union, 43–57.

Webster, S., A. R. Brown, D. R. Cameron, and C. P. Jones, 2003: Improvements to the representation of orography in the Met Office Unified Model. *Quart. J. Roy. Meteor. Soc.*, **129**, 1989–2010, https://doi.org/10.1256/qj.02.133.

White, R. H., D. S. Battisti, and G. H. Roe, 2017: Mongolian mountains matter most: Impacts of the latitude and height of Asian orography on Pacific wintertime atmospheric circulation. *J. Climate*, **30**, 4065–4082, https://doi.org/10.1175/JCLI-D-16-0401.1.

——, ——, and A. Sheshadri, 2018: Orography and the boreal winter stratosphere: The importance of the Mongolian mountains. *Geophys. Res. Lett.*, **45**, 2088–2096, https://doi.org/10.1002/2018GL077098.

Wills, R. C., and T. Schneider, 2015: Stationary eddies and the zonal asymmetry of net precipitation and ocean freshwater forcing. *J. Climate*, **28**, 5115–5133, https://doi.org/10.1175/JCLI-D-14-00573.1.

——, and ——, 2018: Mechanisms setting the strength of orographic Rossby waves across a wide range of climates in a moist idealized GCM. *J. Climate*, **31**, 7679–7700, https://doi.org/10.1175/JCLI-D-17-0700.1.

Yin, J. H., and D. S. Battisti, 2001: The importance of tropical sea surface temperature patterns in simulations of Last Glacial Maximum climate. *J. Climate*, **14**, 565–581, https://doi.org/10.1175/1520-0442(2001)014<0565:TIOTSS>2.0.CO;2.